

The music of marine seismic: A marine vibrator system based on folded surfaces

Okwudili C. Orji¹, Mattias Oscarsson-Nagel¹, Walter Söllner¹, Endrias G. Asgedom¹, Øystein Trætten¹, and Rune Voldsbekk¹

<https://doi.org/10.1190/tle39040254.1>

Abstract

Marine vibrators have bespoke geophysical benefits that are yet to be harnessed because of robustness and efficiency issues. We have developed a new marine vibrator source technology that is efficient and stable. The source technology overcomes the historical problems of inefficiency and robustness by using folded surface technology and resonance frequency tuning. We show measured output examples that demonstrate that the folded surface concept combined with small displacements can provide the required output levels. Our source system consists of a low-frequency module covering 1–10 Hz and a high-frequency module covering 10–125 Hz. The source control system has shown high stability and precision and can handle harmonic distortion. With the aid of synthetic data examples, we demonstrate that seismic data acquired using marine vibrators in either intermittent or continuous mode can be processed. Finally, we demonstrate the environmental friendliness of the source in comparison to air gun-based sources.

Introduction

Seismic data acquisition started on land where explosives were used as sources and quickly developed to using vibrators. The reasons for the quick transition are numerous and include health and safety of personnel and the environment as well as the desire for controlled seismic energy sources. In the marine environment, the operational and environmental consequences of using explosives is higher. In a bid to replace explosive sources in the marine environment, Conoco introduced vibrator sources in the 1960s (Proffitt, 1991). However, air gun sources proved to be more robust and reliable (Chelminski, 1961; Landrø and Amundsen, 2018), and they have since become the industry standard for marine seismic acquisition.

In recent times, the changing geopolitical landscape and technological advances have placed more stringent requirements on the received sound levels from marine seismic sources. The source must be efficient and environmentally friendly and must have sufficient low-frequency output as well as high output fidelity. These requirements are driving the industry to develop alternative source concepts. Marine vibrator sources are a leading candidate among the alternatives (Tenghamn, 2006; Dellinger et al., 2016; Feltham et al., 2018; Roy et al., 2018). In this paper, we discuss the development of one such system — the folded surface marine vibrator (FSMV). We discuss the theoretical background of generating acoustic energy using a marine vibrator and then present practical aspects of building a system that can generate the required energy levels. We then demonstrate specific acquisition scenarios and the processing steps that must be performed. Finally, we

compare the output of the marine vibrator to other air gun-based acquisition methods and demonstrate the advantages of marine vibrators from an environmental perspective.

Main benefits of marine vibrators

Marine vibrators possess a number of unique beneficial capabilities compared to air gun sources. Foremost among these is the nonimpulsive nature of signals generated by marine vibrators, which offers a high degree of control over the output. In contrast, traditional air guns can only generate impulsive signals. This capability provides a number of potential advantages for marine vibrators, including (1) better control of the amplitude and bandwidth of the emitted acoustic energy, which is important for addressing environmental concerns; (2) controlled signal output, which offers opportunities for new and flexible source geometries; and (3) the potential for ultra-low-frequency 1–6 Hz output to benefit full-waveform inversion (Rietsch, 1977; Dellinger et al., 2016; Brenders et al., 2018).

Moreover, marine vibrators are efficient, which in this context is measured by (1) the ratio between the generated acoustic energy and the energy expended and (2) the ratio between the useful energy (effective frequency band) that contributes to imaging the subsurface and the total acoustic energy generated. Conventional air guns require compressed air, which leads to a great deal of energy loss through heat dissipation, whereas electrical conversion to acoustic energy is much more efficient. In addition, much of the acoustic energy generated by air guns contributes energy at frequencies much higher than 250 Hz, which are not typically used for imaging the subsurface. By contrast, marine vibrators can generate tailor-made signatures with whatever frequency content, phase characteristics, and output level is desired. The ability of marine vibrators to generate coded signals can be exploited to mitigate residual shot noise (e.g., Laws et al., 2019) and seismic interference. Furthermore, air guns generate bubble oscillations that can be challenging to remove during processing, whereas marine vibrator signatures can operate with a simple linear sweep.

Generating acoustic energy using marine vibrator elements

In this section, we introduce the theoretical background of generating acoustic energy from vibrating plates in a marine environment. Subsequently, we discuss the relation between the plate motion and the emitted signals and examine the consequences for generating low frequencies.

The basic element of a marine vibrator source is a pair of oscillating plates in water enclosing a volume of air under pressure.

¹PGS, Oslo, Norway. E-mail: okwudili.orji@yahoo.com; mattias.oscarsson-nagel@pgs.com; walter.soellner@pgs.com; endrias.asgedom@pgs.com; oystein.traetten@pgs.com; rune.voldsbekk@pgs.com.

The pressure wavefield outside this volume may be derived from the motion of the vibrator plates caused by an increasing and decreasing enclosed volume (Figure 1).

Starting from the acoustic representation theorem, we consider the pressure wavefield inside the model enclosed by a spherical surface of radius $|r'|$ as the outer border and an idealized surface surrounding the oscillating plates as the inner border. This pressure wavefield is given by:

$$p(\mathbf{x}_R, t) = \int_{S_+ \cup S_-} (g(\mathbf{x}, \mathbf{x}_R, t))^* \nabla p(\mathbf{x}, t) - \nabla g(\mathbf{x}, \mathbf{x}_R, t) \cdot p(\mathbf{x}, t) \cdot ndS \quad (1)$$

where p is the pressure, and g is the free space Green's function that describes propagation from the plate surface to a measuring location \mathbf{x}_R (Morse and Feshbach, 1953).

In equation 1, we have assumed that the surface surrounding the total removed volume is given solely by the plate surfaces S_+ and S_- (i.e., the distance between the plates is much smaller than the plate size). Choosing the direction of the normal vector to point from S_- to S_+ , the integral over the entire surface is:

$$p(\mathbf{x}_R, t) = \int_{S_+} (g(\mathbf{x}, \mathbf{x}_R, t))^* \nabla p(\mathbf{x}, t) - \nabla g(\mathbf{x}, \mathbf{x}_R, t) \cdot p(\mathbf{x}, t) \cdot ndS - \int_{S_-} (g(\mathbf{x}, \mathbf{x}_R, t))^* \nabla p(\mathbf{x}, t) - \nabla g(\mathbf{x}, \mathbf{x}_R, t) \cdot p(\mathbf{x}, t) \cdot ndS \quad (2)$$

So far, no assumptions have been made about the Green's functions or wavefields on the plate surfaces. If we now assume continuity of the pressure fields across the surfaces, which is a valid assumption for thin synchronously oscillating plates separated by a small distance, and impose continuity of the Green's functions and their derivatives across the surfaces, the expression for the pressure reduces to

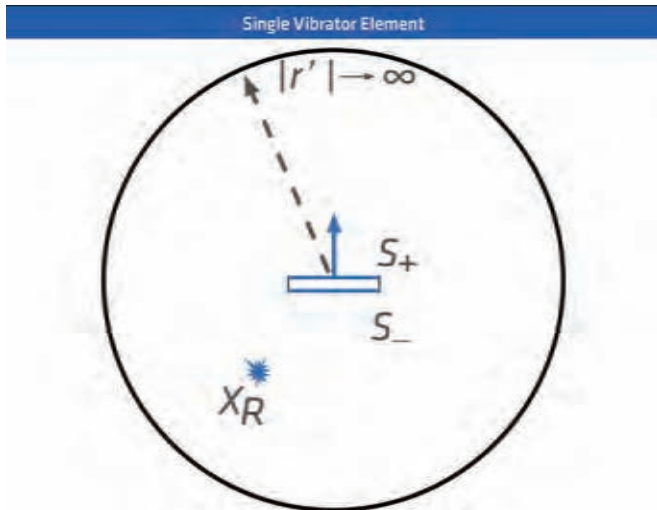


Figure 1. A sketch showing a single vibrator element consisting of a pair of plate surfaces enclosing a volume of air. The normal vector across the inner surface is indicated.

$$p(\mathbf{x}_R, t) = \int_{S_+} g(\mathbf{x}, \mathbf{x}_R, t) \cdot [\nabla p(\mathbf{x}, t)] \cdot ndS \quad (3)$$

The bracket $[\cdot]$ in equation 3 denotes the difference of values — in this case, of the gradients of the pressure wavefield across the plate surfaces. Substituting the pressure gradients in equation 3 by particle velocity \mathbf{v} using $\rho i\omega \mathbf{v} = \nabla p$, we obtain, in the frequency domain,

$$p(\mathbf{x}_R, \omega) = i\omega\rho \int_{S_+} g(\mathbf{x}, \mathbf{x}_R, \omega) [v_n(\mathbf{x}, \omega)] dS \quad (4)$$

where $i\omega v_n$ is the normal component of the plate acceleration, ω is the circular frequency, and ρ is density.

Equation 4 is a general expression for calculating the emitted pressure wavefield everywhere inside the model generated by a pair of synchronously oscillating plates of arbitrary shape. Observe that the pressure wavefield is in phase with the acceleration of the plate oscillation. Consequently, to obtain a flat amplitude spectrum of the far-field pressure emitted by the source, the time function of the plate motion needs to be designed such that the acceleration becomes a flat function in the frequency domain. Generating a flat spectral plate displacement would instead result in an emitted far-field pressure wavefield with the low frequencies suppressed, following $(i\omega)^2$, corresponding to the second time derivative of the signal (Söllner and Orji, 2018). This relation between plate motion and output pressure illustrates the basic challenge of generating low frequencies.

To derive the normal force F_n exerted on the plate surface by a time-harmonic acoustic wavefield, we derive the pressure wavefield at every point on the plate surface from equation 4 and integrate over the surface:

$$F_n \equiv \int_{S_+} p(\mathbf{x}_R, \omega) dS' = i\omega\rho \int_{S_+} \int_{S_+} g(\mathbf{x}, \mathbf{x}_R, \omega) [v_n(\mathbf{x}, \omega)] dS dS' \quad (5)$$

For some simple shaped and rigid plates, equation 5 can be solved analytically for the total force (e.g., Blackstock, 2000):

$$F_n = \pi a^2 v_n \rho c \left[1 - \frac{2J_1(2ka)}{2ka} + j \frac{2K_1(2ka)}{2ka} \right] \quad (6)$$

where, a is the plate radius, k is the wavenumber, and J_1 and K_1 are, respectively, the Bessel and Struve functions of order 1. From the definition of the acoustic impedance, as pressure divided by the particle velocity, the total impedance Z at the plate surface is identified from equation 6 as:

$$Z = \rho c \left[1 - \frac{2J_1(2ka)}{2ka} + j \frac{2K_1(2ka)}{2ka} \right] \quad (7)$$

The real part of the complex radiation impedance is also known as radiation resistance, and the imaginary part is known as radiation reactance. For example, the radiation resistance is a measure of the radiation power, which may be obtained from the real part of the total force in equation 5 or 6 after multiplication by the plate velocity. The volume of water that must be displaced for a desired radiation power can be computed for different frequencies when the vibrator element is acoustically small (i.e., $ka \ll 1$ and the real part of the bracket in equation 6 is expressed by $\frac{(ka)^2}{2}$, the first term of a series expansion). To output significantly more energy at the very low frequencies in comparison to air gun arrays, Figure 2a shows the enormous volume of water that must be displaced per cycle as frequency decreases in order to generate a constant output of 200 dB relative to 1 μPa at 1 m. About 707 liters of water must be displaced at 3 Hz. The required volume of water to be displaced is asymptotically approaching zero and approximately constant starting from about 10 Hz and above. The rapid increase for lower frequencies represents a fundamental physical challenge that applies to any acoustic source deployed in water. For marine vibrators, a consequence is that different engineering approaches must be used to generate frequencies above and below 10 Hz. For this reason, we have chosen to build two specific marine vibrator modules for different frequency ranges: a low-frequency module (LFM) covering 1–10 Hz and a high-frequency module (HFM) covering 10–125 Hz.

A measure of the efficiency of generating acoustic output can be calculated from equation 7 as the ratio of the radiation resistance to the absolute value of the sum of the radiation resistance and the radiation reactance. The efficiency for a unit diameter plate at 10 Hz is 1.2% (see Figure 2b). To overcome this inefficiency, the low-frequency source must be designed such that it resonates at an optimal frequency between 1 and 10 Hz.

The FSMV development

Vibrating membrane design. The opening and closing of an air gun shuttle can be repeated millions of times over a typical lifetime. As soon as the air shuttle opens and closes, the acoustic output is controlled by the surrounding water. Consequently, the sphere of influence is at the beginning of air release, before the passive reaction of water takes over. By contrast, all phases of water motion and sound generation for a marine vibrator are controlled by the membrane of the vibrator. Hence, selection of the size, shape, and material of the membrane are crucial. There are many aspects to consider for successful design of a robust and reliable marine vibrator source.

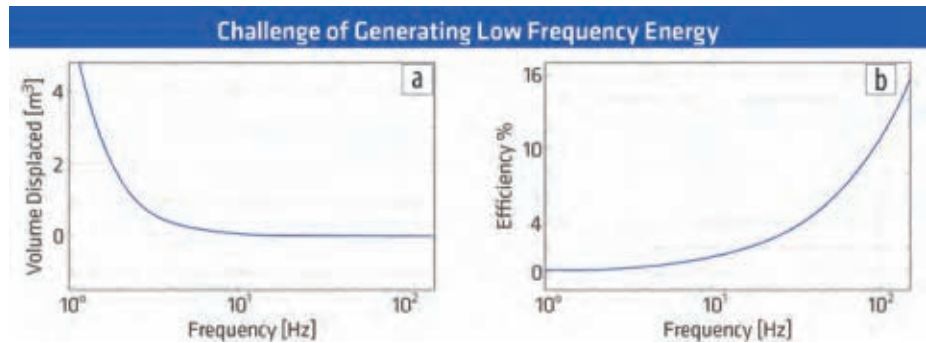


Figure 2. (a) The required volume of water to be displaced per cycle for a constant output of 200 dB relative to 1 μPa @ 1 m. (b) A measure of the efficiency of generating acoustic output as a function of frequency.

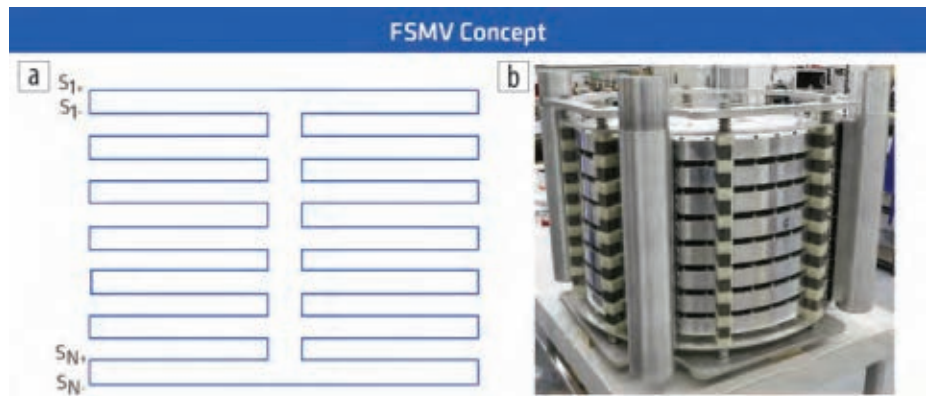


Figure 3. (a) Sketch of the FSMV concept and (b) a picture of the basic element of the prototype.

The material of the membrane may deteriorate over time. It may crack or lose structural abilities, which can eventually lead to leakage and possible failure of the full system. These considerations are especially important when large displacements are used. In addition, marine vibrators are required to vibrate through millions of cycles in their lifetime. Hence, to achieve a robust and reliable design, especially for low-frequency output, small displacements and a large surface area must be used.

Simple calculations can show that source elements with several tens of square meters of effective surface area are unfeasible, especially from an operational point of view. Building a source array comprising many small vibrator elements could generate the desired output level but at very high cost due to the inefficiency of small independent source elements. In our source, the required large surface area is achieved by using a stack of vibrator elements enclosing one common internal volume, leading to an FSMV source. A simplified sketch and picture of the LFM source is shown in Figure 3. The advantage of this design is that the vibrating elements are exposed to lower vibration stresses, which implies a longer service life and lower acoustic distortion compared to alternative designs that use small surface area and large displacements. In addition, the small displacements can be accommodated by a bending metal interface, rather than rolling elastomeric or sliding seal interfaces required by large displacement vibrators.

Resonance frequency tuning. To partially overcome the intrinsic inefficiency of generating low-frequency energy, the LFM unit

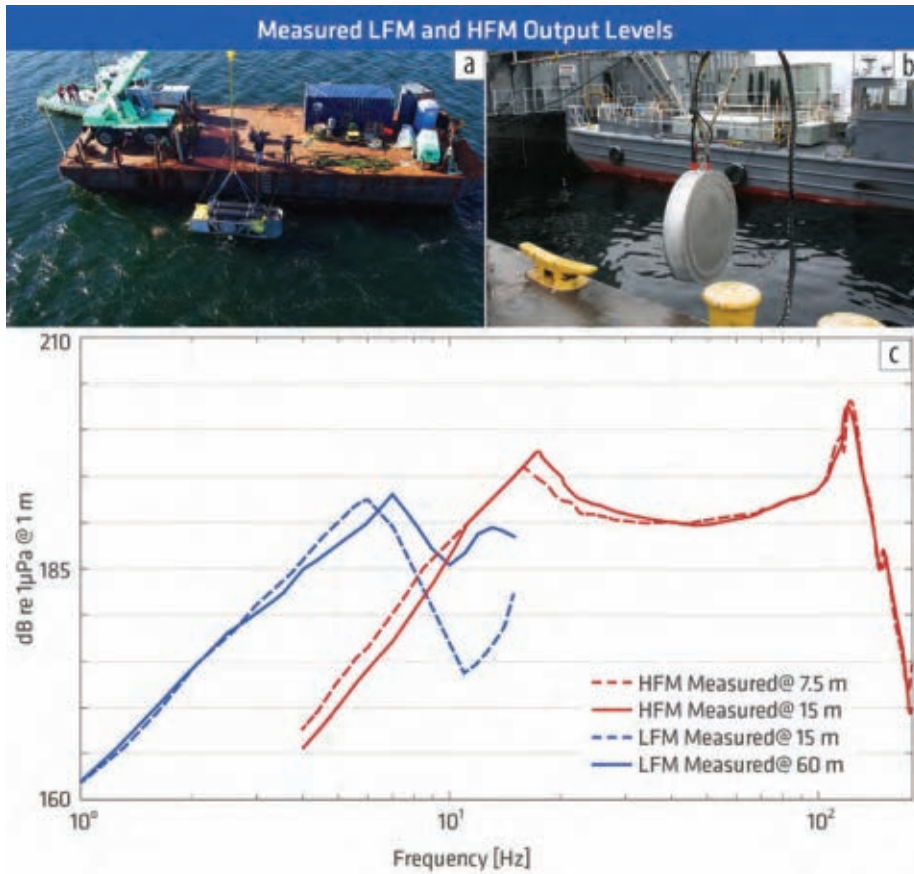


Figure 4. The (a) LFM and (b) HFM at the test site. (c) Measured output levels of the LFM and HFM at different depths.

has been designed to exploit resonance at an optimal frequency between 1 and 10 Hz. At resonance, the source impedance is given by the radiation resistance only (Kinsler et al., 2000). As a rule of thumb, the resonance frequency can be estimated using the mass of the vibrating plate, m_b , the mass of the water vibrating with the plate surface, m_r , the plate stiffness, k_b , and the stiffness of the air trapped between the plates, k_a :

$$f = 1 / 2\pi \sqrt{\frac{(k_b + k_a)}{(m_b + m_r)}} \quad (8)$$

By varying the mass and the stiffness parameters, the resonance frequency can be tuned as desired. One way to achieve this is to stack (or fold) the vibrating plates. By stacking the plates, the resonance frequency decreases. The elastic properties and distances between the vibrator elements are designed based on finite element modeling to produce a controlled resonance of the source in order to increase the output efficiency. The optimal resonance frequency of the LFM was determined to be about 5–7 Hz and was chosen for the deepest depth of 75 m. The resonance frequency and tow depth were chosen considering operational feasibility and safety.

FSMV output characteristics. Prototype modules have undergone multiple sea trials at different operating depths and locations and at various power levels (see Figure 4). Recent efforts have focused on proving operational reliability and scaling up from

single-module calibrations to multi-module full-band exercises. Figure 4c shows the measured output for single modules. The effective output from this prototype is above 190 dB from 4 to 125 Hz. The marine vibrator joint industry project (MV JIP) spectral density level specification is 190 dB re.1 $\mu\text{Pa}/\text{Hz}$ @ 1 m for 5–10 Hz and 200 dB re.1 $\mu\text{Pa}/\text{Hz}$ @ 1 m for 10–100 Hz (e.g., Feltham et al., 2018). However, acoustic output requirements depend on geologic and geophysical challenges and, for many field targets, might be below the MV JIP specifications.

The LFM unit was tested at 15 and 60 m depth, while the HFM unit was tested at 7.5 and 15 m depth. The change in resonance frequency is related to the increasing air stiffness with depth. The resonance frequency of the HFM unit is optimized for shallow depths, while that of the LFM unit is optimized for deep tow. Towing the LFM units shallower is beneficial because the resonance moves to lower frequencies, and it is also convenient since it is operationally more challenging to tow deeper. However, this benefit must be traded off against the geophysical advantages

of a deep towed source to exploit the effect of constructive interference with the source ghost at low frequencies. Unity chirp rate is required to achieve the output levels shown in Figure 4c (for linear sweeps). The implication is that the sweep length required will affect source point sampling at normal acquisition speeds, which will be discussed in a later section. Figures 5a and 5b show plots of the computed 5 s output for two LFM and four HFM units. The output of the system for 5 s is above 180 dB for the frequencies covering 1–125 Hz. The computed signatures are based on predicted source levels.

Timing and phase control. A central benefit of marine vibrators is that they are controllable. Hence, the transducers and the control system must be stable and show high fidelity. To achieve this, the combined transfer function of the transducers and the control system must be repeatable such that it can be accounted for during signal generation. Figure 6 shows measured output from the HFM unit. To demonstrate the timing accuracy and stability of the system, 10 continuous linear sweeps with randomized lengths ranging from 4 to 6 s covering 10–80 Hz were tested. The source was operated in both continuous (Figure 6a) and intermittent (Figure 6b) modes. In continuous mode, the continuous sweep was repeated several times by allowing different time intervals between each sequence. In intermittent mode, a fixed time interval (20 s) was allowed between each sweep. The red dots indicate the required (reference) trigger times of the source. The trigger time error is computed as the difference between the commanded

trigger times (reference) and the measured trigger times. The computed error is far less than 1 ms (Figure 6c).

A further demonstration of source control is to verify the ability of the source to generate pseudorandom signals. In general, pseudorandom signals are more difficult to generate compared to linear sweeps due to the near random phase of the signals. Figure 7a shows plots of two pseudorandom signals emitted at different times. Figure 7b shows a 1 s zoom of Figure 7a, and Figure 7c shows a plot of the first shot overlaid with the scaled control signal. The two signals are in phase, which demonstrates the controllability and fidelity of the system.

Harmonic distortion. When marine vibrators are operated with large displacements, they generate high harmonic distortion levels. The level of harmonic distortion is generally related to the total stiffness of the source. When the air inside the source is very stiff and large displacements are used, nonlinear performance occurs leading to high harmonic distortion. In addition, the distortion levels increase when the source is operated near or at its resonance frequency. Operating the source above the resonance frequency generates low levels of harmonic distortion. Figure 8a shows a spectrogram of the output in Figure 6a. There is little or no harmonic distortion, which demonstrates that the HFM unit is inherently a low-distortion system. However, the output of the LFM unit (Figures 8b and 8c) shows some harmonic distortion as expected. Increasing the depth of operation of the unit increases the air stiffness, which leads to more harmonic distortion (compare Figures 8b and 8c). To counteract this phenomenon, the source system has active distortion-reduction algorithms such as iterative learning control (ILC). Figure 8d shows a spectrogram of an LFM output with ILC applied for harmonic attenuation and clearly exhibits reduced levels of harmonic distortion.

Towing and handling. The FSMV is modular and consists of a few modules combined in tow bodies (sleds). The sleds can either be connected to a surface float as in conventional source systems

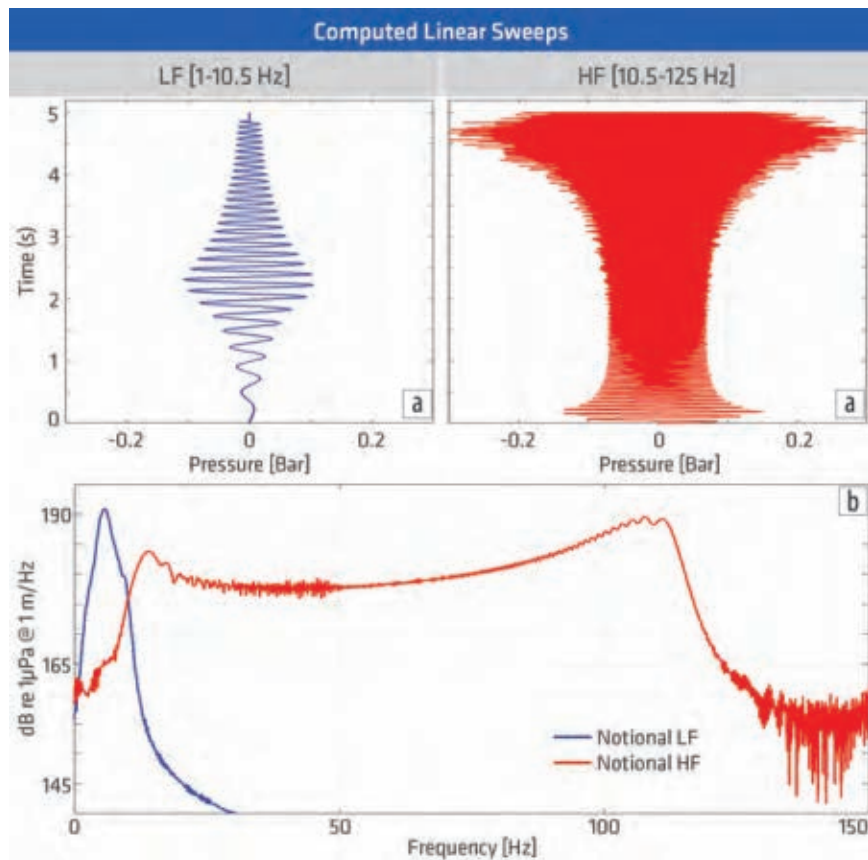


Figure 5. (a) Time plots and (b) frequency spectra. Computed 5 s linear sweeps based on the predicted output levels for two LFM units covering 1–10 Hz (blue) and four HFM units covering 10–125 Hz (red).

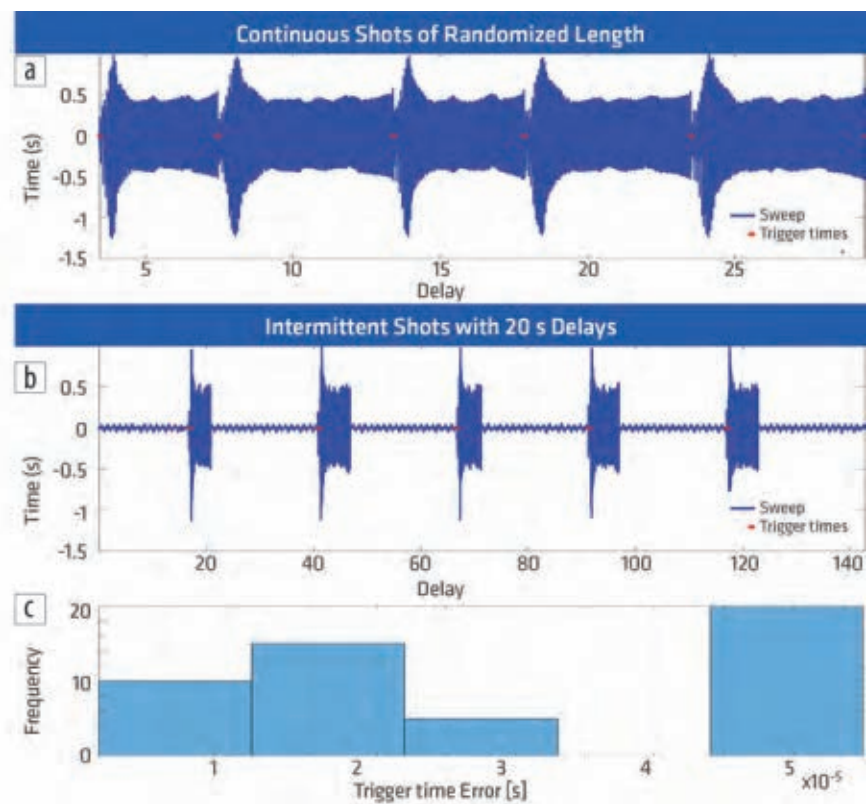


Figure 6. Measured HFM data for randomized sweeps in (a) continuous emission and (b) intermittent mode. (c) Histogram of the computed triggering time errors.

or towed directly from the body with built-in individual depth control. The system is designed to utilize existing vessel equipment as much as possible to facilitate a cost-efficient technology

introduction. A key design focus of the overall system is seamless integration into the existing seismic vessel back-deck configuration envelope. These requirements place constraints on the overall size, weight, and output levels of the system.

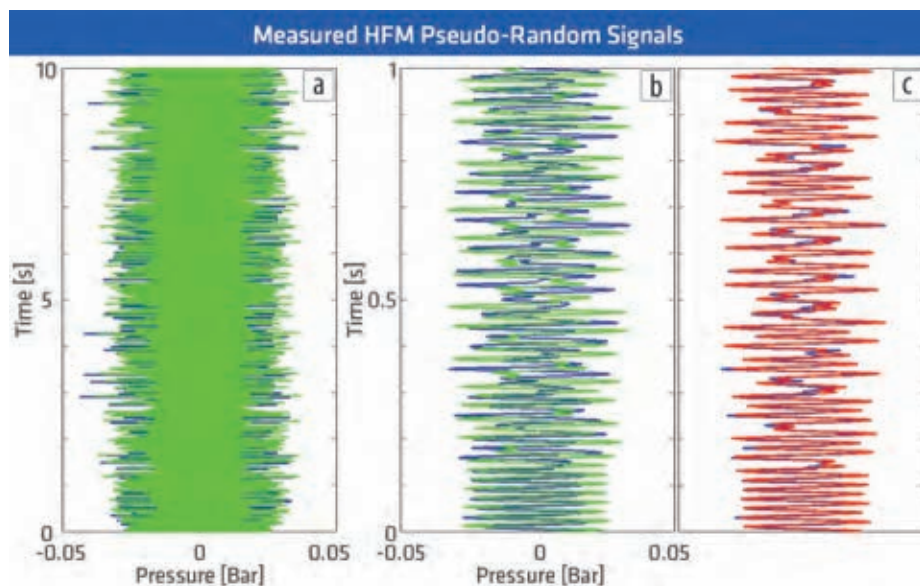


Figure 7. (a) Measured HFM pseudorandom signals repeated two times, (b) a 1 s zoom of the plots in (a), and (c) the first measured signal plotted with the scaled control signal.

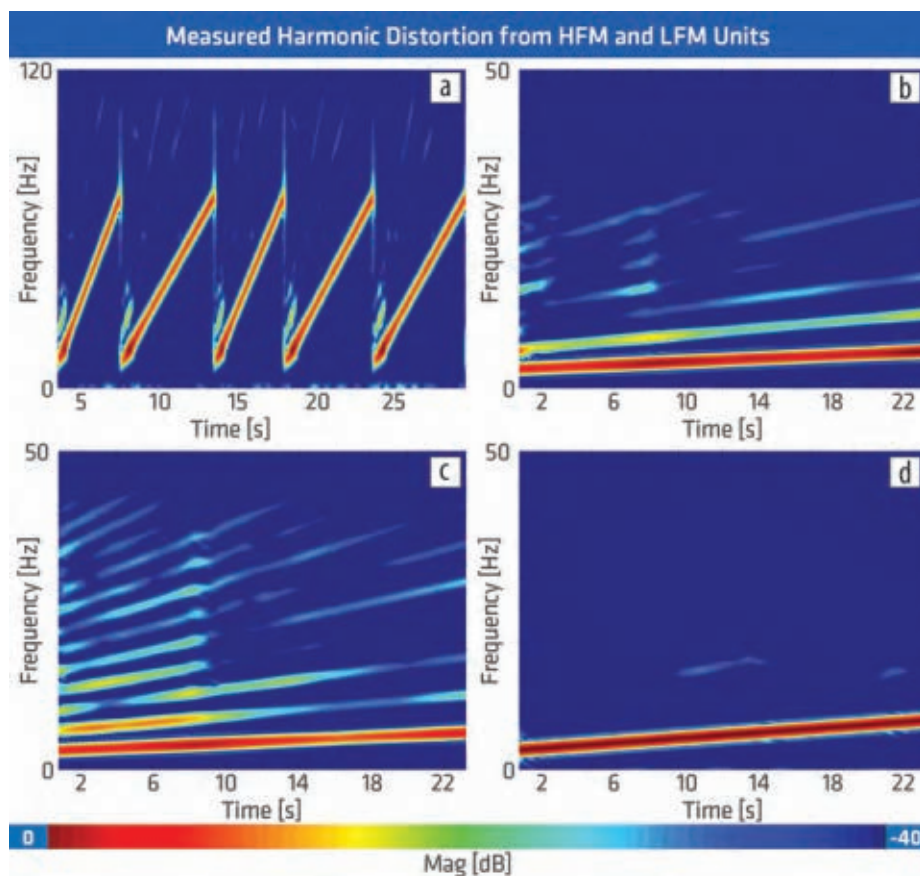


Figure 8. Spectrograms measured for different marine vibrator elements. (a) HFM continuous signal (shown in the left plot of Figure 6a). (b) LFM deployed at 15 m depth for a 24 s linear sweep covering 3–6 Hz. (c) LFM deployed at 60 m depth for the same sweep. (d) LFM with active distortion reduction applied for a 20 s, 3–8 Hz sweep when the source is deployed at 15 m depth.

The deployment and recovery capability, using existing methods, must be balanced with optimal vessel back-deck space utilization of the current marine seismic source system. These have to function in a safe and reliable manner, including in marginal sea conditions. The number of LFM and HFM units that are configured into sleds, and the required number of sleds, will fit within the current marine seismic vessel back deck. Hence, the commercial system will require minimal adjustment of the existing marine seismic vessel back-deck layout and can be seamlessly integrated into existing seismic vessel platforms.

Source separation is typically limited to 50–200 m for conventional seismic acquisition using air guns. This narrow towing configuration is limited by the specifications of the umbilical cable. This has implications for acquisition efficiency since increased source separation opens the possibility for increased sail line separation, meaning a given survey area could be covered in a shorter time. The FSMV is an electrical system and, although pressure compensation is required, the specification of the umbilical cable for the full system will allow for wider towing configurations subject to other operational limits. In the future, the sleds could be self-contained unmanned vessels with integrated propulsion and power supply systems. This concept would eliminate the limitation on tow width.

Continuous versus intermittent acquisition: Synthetic examples

The ability to control marine vibrator output offers versatility in terms of survey design. Traditional intermittent emission and listening for a given time interval is suitable for air gun arrays since the air compressors need time to recharge. Some marine vibrators must be operated at 50% duty cycle due to limitations inherent in their design (e.g., overheating due to large displacements), and, for these designs, acquisition must also be performed in an intermittent manner similar to air gun acquisition. The FSMV does not suffer

this limitation, which means the vibrator can be operated continuously if so desired. In this section, the implications of intermittent and continuous acquisition will be explored.

A synthetic data modeling and processing exercise was performed to evaluate different acquisition and processing solutions. Data examples were modeled using finite difference modeling for the Sigsbee 2B model. The source signatures used in modeling were prepared using the predicted output from Figure 5. For intermittent acquisition, the length of the signature was 5 s with 5 s of listening time. The source and the receivers were modeled as moving with a speed of 2.5 m/s at depths of 10 and 20 m, respectively, giving a shot point interval of 25 m. The temporal sampling interval was 4 ms with 12.5 m receiver spacing. The source wavefield containing the source motion is shown in Figure 9a.

To remove the effects of the source signature, trace-by-trace correlation with the far-field signature (pilot sweep) was performed. Figures 9b and 9c show the total pressure shot record before and after this correlation. Observe that, after the correlation, the resulting data in Figure 9c resemble seismic data from an impulsive source. Consequently, further data processing flows that are routinely applied to air gun data can be used from this point onward.

The primary difference between data acquired with air guns compared to that from a marine vibrator is the effect of source motion. An air gun emits energy at a single point in space, which can be assumed to be stationary. For a marine vibrator, the point at which energy is emitted is constantly changing as the source moves through the water. The processing demonstrated in Figure 9 neglects the effect of this source motion yet still yields a reasonable

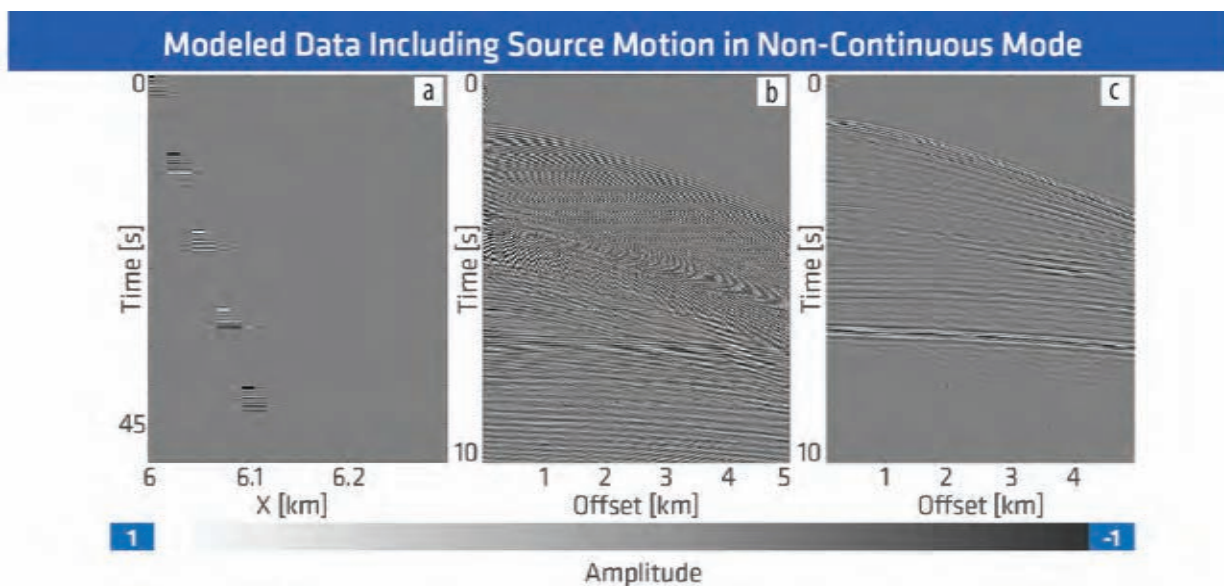


Figure 9. (a) The modeled source wavefield including the source motion for a FSMV source system used in intermittent mode. (b) The modeled total pressure wavefield obtained from this source for a single sweep. (c) The total pressure wavefield after crosscorrelation with the pilot sweep.

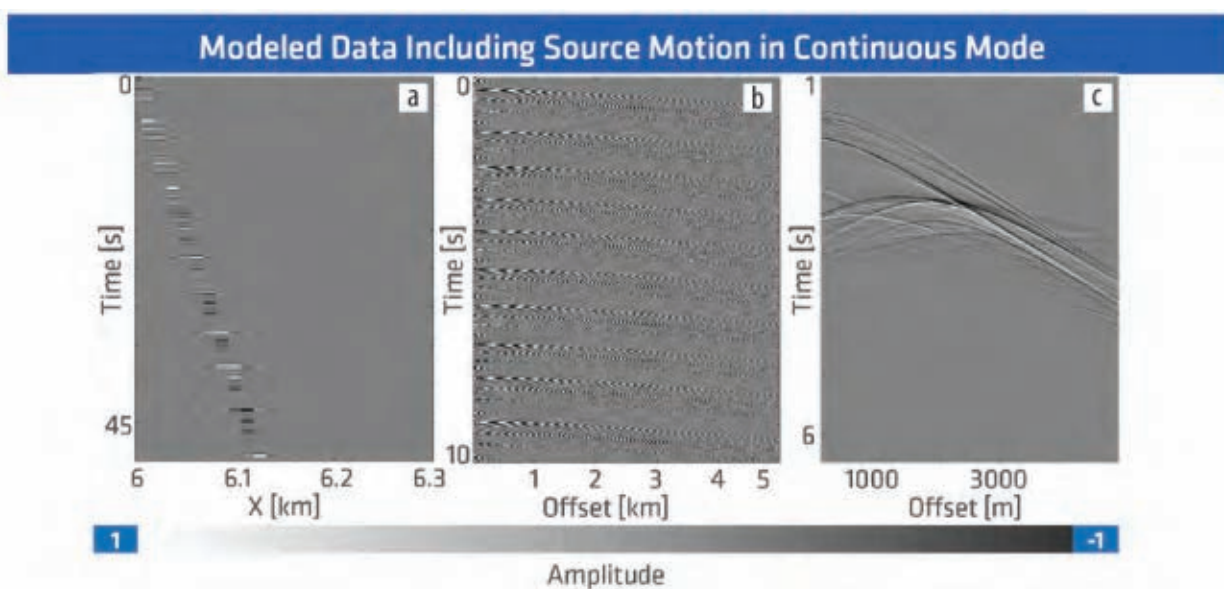


Figure 10. (a) The modeled source wavefield including the source motion for a FSMV system used in continuous mode. (b) The modeled continuous total pressure wavefield. (c) The ongoing pressure wavefield after source wavefield deconvolution.

result. Methods for correcting for source motion have been demonstrated (e.g., Dragoset, 1988; Hampson and Jakubowicz, 1995; Asgedom et al., 2019). This source motion correction must be applied in the common-receiver domain. Consequently, when marine vibrators are used to acquire data in an intermittent manner, spatial aliasing limits the possibility of applying a proper motion source correction. For the shot point interval of 25 m used in Figure 9, spatially unaliased signal can only be obtained up to 30 Hz. If the shot point interval were reduced to 12.5 m to partially mitigate this aliasing problem, the time interval between two shots would be 5 s, which is the length of the actual sweep resulting in blending of the data from successive sweeps.

The most efficient method for exploiting the full benefits of marine vibrators is to use them in continuous emission mode. Such acquisition will remove the spatial sampling limitations that arise from intermittent acquisition. The FSMV source system can emit signals that approximate the characteristics of band-limited white noise, which is the theoretically ideal continuous signal. This can be achieved by operating the source at 100% duty cycle (e.g., Figure 6a). A processing methodology that utilizes continuous wavefields on both the source and the receiver sides has been developed and demonstrated using an air gun source (Hegna et al., 2018). The same principles can be applied to continuous marine vibrator data.

Using the same data acquisition configuration as in Figure 9, data were modeled using a continuous wavefield (see Figure 10a). The randomized sweep length is from 4 to 6 s. The first 50 s of the continuous total pressure data is shown in Figure 10b. The effect of the continuous wavefield can be deconvolved following Hegna et al. (2019) (Figure 10c). The deconvolution removes all source motion effects and performs source deghosting and designature of the data. As in the case of intermittent acquisition, the output resembles impulsive data and can be processed similarly.

Environmentally friendly seismic sources

The risk of potential harm and disturbance of marine life due to actuation of marine seismic sources is routinely assessed before carrying out any marine seismic survey. The two commonly used environmental metrics to assess the received sound levels are the peak sound pressure level (pSPL) and the sound exposure level (SEL). The pSPL is related to the maximum output of the source in the time domain, while the SEL is related to the total energy output of the source. The marine seismic industry is moving toward data acquisition methods that are more environmentally friendly using various techniques, including lower source output levels (e.g., Laws et al., 2017; Klüver et al., 2018), improved data acquisition

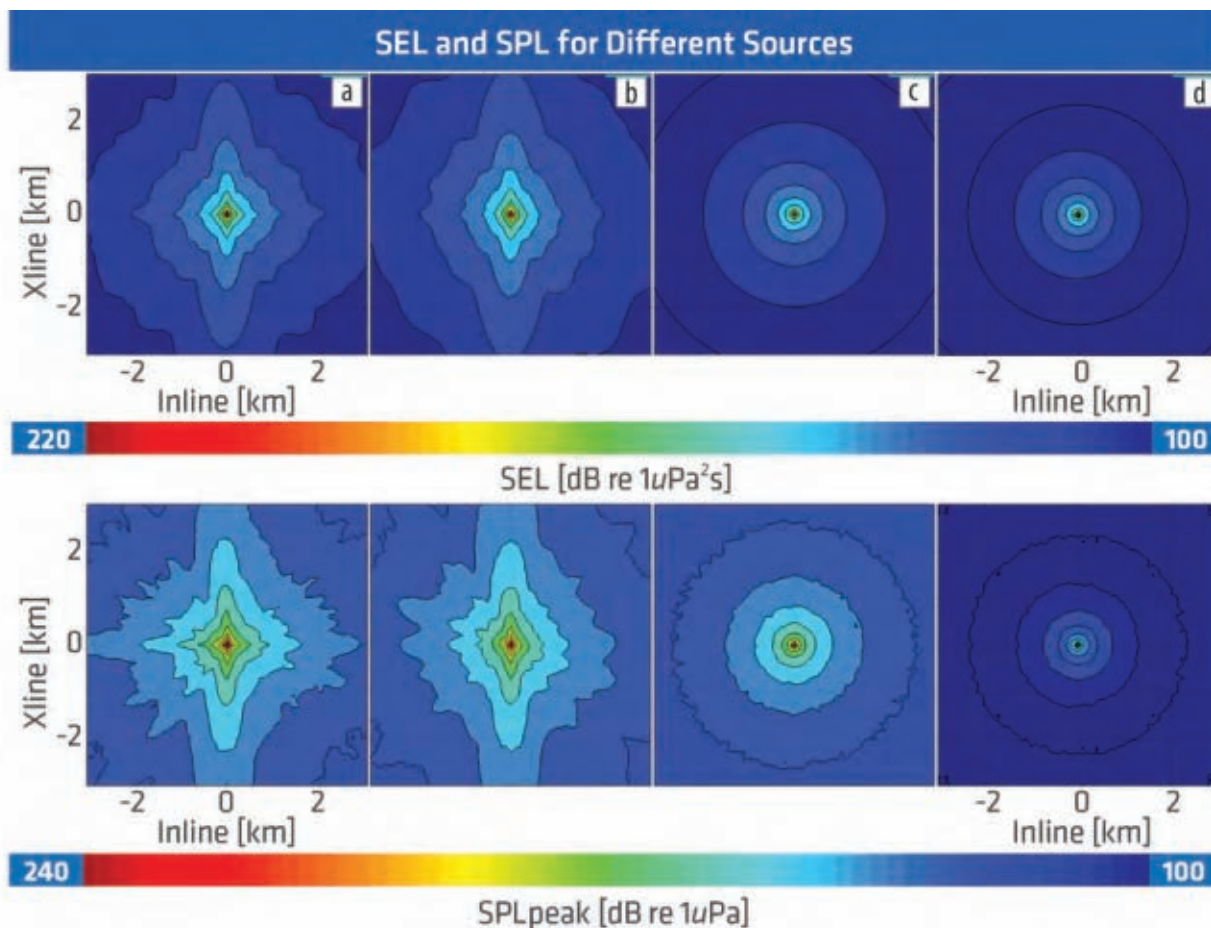


Figure 11. The emitted SEL (top panels) and pSPL (lower panels) for different sources. (a) A 4130 in³ air gun array with 10 s shot interval. (b) A 3280 in³ air gun array with 7.5 s shot interval. (c) Single-string continuous shooting air gun source. (d) PGS MV prototype used in continuous emission and recording mode. The recording time window considered is 10.5 s.

techniques (Abma, 2018; Hegna et al., 2018), new source technology (e.g., Laws et al., 2017; Orji et al., 2019), or a combination of the three (Hegna et al., 2019). The challenge is to achieve these goals without compromising data quality.

The output of different seismic sources used in different acquisition modes was modeled to assess their environmental impact. In the comparison, all the air gun sources were modeled at 6 m depth, while the marine vibrators were modeled at 10 m depth. The frequency band between 0 Hz and 1 kHz was considered for all sources; however, note that the marine vibrator source only delivers seismic energy between 1 and 100 Hz. The recording time window length considered is 10.5 s, and only the direct arrival and its ghost contributions were modeled from the sources to their corresponding receivers located 1 m below the source.

Figure 11 shows the SEL (top panels) and pSPL (bottom panels) as a function of lateral displacement from the source for four different acquisition scenarios. Figure 11a shows the computed SEL and pSPL for a 4130 in³ air gun array, representative of dual-source acquisition fired every 10 s. Observe the directivity pattern related to the spatial configuration of the array, which comprises three subarrays. Figure 11b shows the results for a 3280 in³ air gun source, representative of a two-subarray source used for triple-source acquisition fired every 7.5 s. The 3280 in³ array shows a reduction of approximately 2.5 dB in SEL and approximately 4.5 dB in pSPL at vertical incidence relative to the 4130 in³ array. Despite the reduction in volume, the reduction in sound output is modest due to the reduced firing interval. Figure 11c shows the SEL and pSPL for continuous shooting for one string with 40, 90, and 150 in³ air guns fired randomly in time with an average interval of 292 ms (Hegna et al., 2018). The SEL and pSPL results in a reduction of approximately 10 and 14 dB relative to the 4130 in³ air gun array at the vertical incidence direction, respectively.

Finally, the modeled output from the FSMV prototype used in continuous shooting mode is shown in Figure 11d. Observe the omnidirectional behavior of both air gun and marine vibrator sources used in continuous shooting mode. Table 1 shows the summary of the output levels of the sources at 0.5 km exclusion zones. In terms of pSPL, which has been associated with physiological damage to marine mammals (NOAA, 2016), the FSMV has by far the lowest output. If the calculations are limited to the bandwidth used for seismic imaging (0–100 Hz), Table 1 shows that the SEL of the FSMV is comparable to the output level of the air gun sources, which indicates that a similar image quality could be expected.

Conclusions

Marine vibrators have many promising geophysical benefits, but they are yet to demonstrate robustness and reliability. Using knowledge of the physical laws that describe acoustic energy generation in water, we developed two marine vibrator systems that operate at the low- and high-frequency ends of the seismic frequency bands. The marine vibrator design uses large surface

Table 1. Summary of the environmental metrics at 0.5 km exclusion zone in the inline direction.

Inline	4130 in ³	3280 in ³	Air gun continuous	FSMV continuous
SEL[dBre1μPa2s] full band	145.02	143.96	133.74	127.68
SEL[dBre1μPa2s] 0–100 Hz	140.6	140.38	126.97	127.68
pSPL[dBre1μPa] full band	170.46	166.57	158.23	126.39
pSPL[dBre1μPa] 0–100 Hz	162.71	158.61	142.66	126.39

area and small displacements to achieve robustness and reliability. The source exploits resonance tuning to improve efficiency, especially at low frequencies where the efficiency challenges are greatest for all marine seismic sources. We have demonstrated that the full-source system is stable and can employ active harmonic distortion if required. Using synthetic data examples, we have shown the implications for processing marine vibrator data. Finally, we have demonstrated the environmental friendliness of the source compared to air gun sources. **TIE**

Acknowledgments

We are grateful to PGS for permission to publish this work. Special thanks to Luka Baranic, Anthony Day, and all of our PGS colleagues for support and many useful discussions. We thank the team at GeoSpectrum Technologies Inc., Canada.

Data and materials availability

Data associated with this research are confidential and cannot be released.

Corresponding author: okwudili.orji@yahoo.com

References

- Abma, R., 2018, Shot coding design for popcorn shooting: 88th Annual International Meeting, SEG, Expanded Abstracts, 56–60, <https://doi.org/10.1190/segam2018-2995736.1>.
- Asgedom, E. G., O. C. Orji, and W. Söllner, 2019, Marine vibrator sources: Motion correction, deghosting and designation: 81st Conference and Exhibition, EAGE, Extended Abstracts, <https://doi.org/10.3997/2214-4609.201901411>.
- Blackstock, D. T., 2000, Fundamentals of physical acoustics: John Wiley & Sons Inc.
- Brenders, A., J. Dellinger, C. Kanu, Q. Li, and S. Michell, 2018, The Wolfspär field trial: Results from a low-frequency seismic survey designed for FWI: 88th Annual International Meeting, SEG, Expanded Abstracts, 1083–1087, <https://doi.org/10.1190/segam2018-2996201.1>.
- Chelminski, S., 1961, Acoustic wave impulse generator repeater: U.S. Patent 3249177A.
- Dellinger, J., A. Ross, D. Meaux, A. Brenders, G. Gesoff, J. Etgen, J. Naranjo, G. Openshaw, and M. Harper, 2016, Wolfspär, an “FWI-friendly” ultralow-frequency marine seismic source: 86th Annual International Meeting, SEG, Expanded Abstracts, 4891–4895, <https://doi.org/10.1190/segam2016-13762702.1>.
- Dragoset, W. H., 1988, Marine vibrators and the Doppler effect: Geophysics, **53**, no. 11, 1388–1398, <https://doi.org/10.1190/1.1442418>.
- Feltham, A., M. Jenkerson, N. Henderson, M. Girard, V. Nechayuk, and A. Cozzens, 2018, Geophysical testing of a marine vibrator integrated projector node (MV-IPN) at Seneca Lake: 80th Conference

- and Exhibition, EAGE, Extended Abstracts, <https://doi.org/10.3997/2214-4609.201800996>.
- Hampson, G., and H. Jakubowicz, 1995, The effects of source and receiver motion on seismic data: *Geophysical Prospecting*, **43**, no. 2, 221–244, <https://doi.org/10.1111/j.1365-2478.1995.tb00133.x>.
- Hegna, S., T. Klüver, and J. Lima, 2018, Making the transition from discrete shot records to continuous wavefields — Methodology: 80th Conference and Exhibition, EAGE, Extended Abstracts, <https://doi.org/10.3997/2214-4609.201800998>.
- Hegna, S., T. Klüver, O. Orji, and J. Lima, 2019, The continuous wavefields method: Using electro-mechanical sources: 89th Annual International Meeting, SEG, Expanded Abstracts, 4019–4023, <https://doi.org/10.1190/segam2019-3209867.1>.
- Kinsler, L. E., A. R. Frey, A. B. Coppens, and J. V. Sanders, 2000, *Fundamentals of acoustics*, 4th edition: John Wiley & Sons Inc.
- Klüver, T., S. Hegna, and J. Lima, 2018, Making the transition from discrete shot records to continuous wavefields — Real data application: 80th Conference and Exhibition, EAGE, Extended Abstracts, <https://doi.org/10.3997/2214-4609.201800999>.
- Laws, R., D. Gerez, C. Ocampo, M. Supawala, and L. Na, 2017, A comparison of image quality and potential environmental impact for two types of air gun: 87th Annual International Meeting, SEG, Expanded Abstracts, 101–105, <https://doi.org/10.1190/segam2017-17674813.1>.
- Laws, R. M., D. Halliday, J.-F. Hopperstad, D. Gerez, A. Supawala, A. Özbek, T. Murray, and E. Kragh, 2019, Marine vibrators: The new phase of seismic exploration: *Geophysical Prospecting*, **67**, no. 6, 1443–1471, <https://doi.org/10.1111/1365-2478.12708>.
- Landrø, M., and L. Amundsen, 2018, Marine vibrators, part I: *Geo ExPro*, **15**, no. 3, 52–53.
- Morse, P. M., and H. Feshbach, 1953, *Methods of theoretical physics: McGraw-Hill Book Comp.*
- NOAA, 2016, Technical guidance for assessing the effects of anthropogenic sound on marine mammal hearing — Underwater acoustic thresholds for onset of permanent and temporary threshold shifts: NOAA Technical Memorandum NMFS-OPR-55.
- Orji, O., M. D. C. Oscarsson-Nagel, W. Söllner, Ø. Trætten, B. Armstrong, D. Nams, and P. Yeatman, 2019, Marine vibrator source: Modular projector system: 89th Annual International Meeting, SEG, Expanded Abstracts, 52–56, <https://doi.org/10.1190/segam2019-3215325.1>.
- Proffitt, J. M., 1991, A history of innovation in marine seismic data acquisition: *The Leading Edge*, **10**, no. 3, 24–30, <https://doi.org/10.1190/1.1436807>.
- Rietsch, E., 1977, Computerized analysis of vibroseis signal similarity: *Geophysical Prospecting*, **25**, no. 3, 541–552, <https://doi.org/10.1111/j.1365-2478.1977.tb01186.x>.
- Roy, D. A., R. Rekos, C. Brideau, T. Lawry, and C. Corrada, 2018, A marine vibrator to meet the Joint Industry Project specification: 88th Annual International Meeting, SEG, Expanded Abstracts, 97–101, <https://doi.org/10.1190/segam2018-2997347.1>.
- Söllner, W., and O. C. Orji, 2018, Marine vibrator source acceleration and pressure: US 2018/0052245 A1.
- Tenghamn, R., 2006, PGS shows off electrical marine vibrator to capture ‘alternative’ seismic source market: *First Break*, **24**, no. 1, 33–36.



Let SEG help navigate your road to improvement.

SEG Competency Management System

A free benefit for SEG members, the SEG Competency Management System (CMS) helps you identify new learning opportunities and manage your career. Designed to easily identify competency gaps based on assessment results, the software recommends a learning plan that helps close these gaps. Find out more at seg.org/cms.

CMS learning plans include SEG training resources such as eLearning courses, third party course titles, SEG technical papers, books, and more. **For a limited time, SEG is offering \$25 off all IHRDC courses at seg.org/ondemand, and when you buy 6 modules of Leon Thomsen’s Geophysics 101 course you’ll get the 7th free.** To take advantage of the Geophysics 101 course offer, email cjackson@seg.org.

seg.org/education